-Referee#3-

We appreciate you for the valuable and insightful comments, which have greatly improved our manuscript. Below we describe the modifications made according to the comments. For clarity, comments are given in italics and blue, and our responses are given in plain text. The line numbers within brackets indicate the location of the modifications in the revised manuscript. The revised manuscript with all revisions tracked is appended at the end of this document.

> *The nonstationarity of the runoff in Wei River basin is very significant and this work applied multiple variables into time-varying model by GLM. The revised version addressed the comments of the last two referees clearly.*

AUTHORS' REPONSE: We appreciate you very much for your positive comment.

> *Line 26 and the others, "potential evapotranspiration, ET". Usually, ET is used to represent actual evapotranspiration and EP is used to represent potential evapotranspiration. It's better to use EP to represent potential evapotranspiration.*

AUTHORS' REPONSE: Thank you for pointing out this. To address your comment, "ET" and "AI_{ET}" have been modified as "EP" and "AI_{EP}", respectively.

> *Irrigated area is a very important index in the Wei River due to large agricultural irrigation water withdrawn. And irrigated area is added in the revised version.*

AUTHORS' REPONSE: We quite agree with your comment.

> *Line 345-348, "Human activity data(i.e. gross domestic product, population and irrigation area) were taken from annals of statistics provided by the Shaanxi Provincial Bureau of Statistics (http://www.shaanxitj.gov.cn/) and Gansu Provincial Bureau of Statistics (source: http://www.gstj.gov.cn/)." If the data also come from Zhang (2008) as shown in Line 326, it should be listed here.*

AUTHORS' REPONSE: Thank you for your good comment. We realize that this is our negligence. After the first revision, the Line 324-326, "In this study, we use the available data (1980-2005) of the irrigation diversion system on plateau in Baoji Gorge Irrigation Area in Zhang (2008) to provide some information for the knowledge of low flow generation", should have been deleted. And we have deleted this sentence in the revised manuscript. This is because human activity data in the annals is more detailed than the data in Zhang (2008). As also the referee 2 suggested, the shorted records in Zhang (2008) is limited for this study. Thus, after first revision, the data in Zhang (2008) was replaced by the data (1954-2009) in the annals.

> *It should be noted that the "population" in the annals are different from the people who lives in the catchment. So the uncertainty should be presented here to remind the readers. Nonetheless, it is the best population data so far.*

AUTHORS’ REPONSE: We are grateful for your insightful suggestion. We have added following sentence to Sect.4.3 Discussion:

“Besides, it should be noted that the "population" recorded in the annals of statistics may not be equal to the actual population living in the catchment. If the “population” in the annals is used as explanatory variable, this difference may lead to uncertainty of model parameter estimations. Nonetheless, it is the best population data so far and the explanatory variable POP is excluded in the final model (M6).” [Lines 504-508]

Multiple Causes of Nonstationarity in the Weihe Annual Low Flow Series

Bin Xiong[1], Lihua Xiong[1*], Jie Chen[1], Chong-Yu Xu[1, 2], Lingqi Li[1]

1 State Key Laboratory of Water Resources and Hydropower Engineering Science, Wuhan University, Wuhan 430072, P.R. China

2 Department of Geosciences, University of Oslo, P.O. Box 1022 Blindern, N-0315 Oslo, Norway

* *Corresponding author:*

Lihua Xiong, PhD, Professor

State Key Laboratory of Water Resources and Hydropower Engineering Science

Wuhan University, Wuhan 430072, P.R. China

E-mail: xionglh@whu.edu.cn

Telephone: +86-13871078660

Fax: +86-27-68773568

Abstract:

Under the background of global climate change and local anthropogenic activities, multiple driving forces have introduced various non-stationary components into low-flow series. This has led to a high demand on low-flow frequency analysis that considers nonstationary conditions for modeling. In this study, through a nonstationary frequency analysis framework with the Generalized Linear Model (GLM) to consider time-varying distribution parameters, the multiple explanatory variables were incorporated to explain the variation in low-flow distribution parameters. These variables are comprised of the three indices of human activities (i.e., population *POP*, irrigation area *IAR*, and gross domestic product *GDP*) and the eight measuring indices of the climate and catchment conditions (i.e., total precipitation *P*, mean frequency of precipitation events λ, temperature *T*, potential evapotranspiration *EP*~~*ET*~~, climate aridity index AI_{EP}~~AI_{ET}~~, base-flow index *BFI*, recession constant *K* and the recession-related aridity index AI_K). This framework was applied to model the annual minimum flow series of both Huaxian and Xianyang gauging stations in the Weihe River, China. The results from stepwise regression for the optimal explanatory variables show that the variables related to irrigation, recession, temperature and precipitation play an important role in modeling. Specifically, analysis of annual minimum 30-day flow in Huaxian shows that AI_K is of the highest relative importance among the optimal variables, followed by *IAR*, *BFI* and AI_{EP}~~AI_{ET}~~, and nonstationary GA distribution model with these optimal

variables has an AIC value of 207.0, while the AIC values of other models just with AI_K or time as explanatory variable or without any variable are 217.4, 225.5, 232.3, respectively. We conclude that the incorporation of multiple indices related to low-flow generation permits tracing various driving forces. The established link in nonstationary analysis will be beneficial to analyze future occurrences of low-flow extremes in similar areas.

Keywords: Climate Change; Streamflow Recession; Multiple Factors; Nonstationarity; Low-flow Frequency Analysis;

1. Introduction

Low flow is defined as the ‘flow of water in a stream during prolonged dry weather’ (WMO, 1974). Yu et al. (2014) quantitatively described a low flow event as a segment of hydrograph during a period of dry weather with discharge values below a preset (relatively small) threshold. According to WMO (2009), annual minimum flows averaged over several days can be used to measure low flows. During low-flow periods, the magnitude of river flow will greatly restrict its various functions (e.g. providing water supply for production and living, diluting waste water, ensuring navigation, meeting ecological water requirement). Therefore, the investigation of the magnitude and frequency of low flows is of primary importance for engineering design and water resources management (Smakhtin, 2001). In recent years, low flows, as an important part of river flow regime, have been attracting an increasing attention of hydrologists and ecologists in the context of the significant impacts of climate change and human activities (Bradford and Heinonen, 2008; Du et al., 2015; Kam and Sheffield, 2015; Kormos et al., 2016; Liu et al., 2015; Sadri et al., 2015; Smakhtin, 2001; WMO, 2009). In general, under the impact of a changing environment, combinations of multiple factors, such as precipitation change, temperature change, irrigation area change and construction of reservoirs, can drive various patterns of streamflow changes (Liu et al., 2017; Tang et al., 2015). Unfortunately, when subjected to a variety of influencing forces, low flow is more vulnerable than high flow or mean flow. Therefore, it is a pretty important issue in hydrology to identify low-flow changes, track multiple driving factors and quantify their contributions from the perspective of hydrological frequency analysis.

In hydrological analysis and design, conventional frequency analysis estimates the statistics of a hydrological time series based on recorded data with the stationary hypothesis which means that this series is “free of trends, shifts, or periodicity (cyclicity)” (Salas, 1993). However, global warming and human forces have changed climate and catchment conditions in some regions. Time-varying climate and catchment conditions can affect all aspects of the flow regime, i.e. changing the frequency and magnitude of floods, altering flow seasonality, and modifying the characteristics of low flows, etc. The hypothesis of stationarity has been suspected (Milly et al., 2008). If this problematic method is still used, the frequency analysis may lead to high estimation error in hydrological design. Therefore, considerable literatures have introduced the concept of hydrologic nonstationarity into analysis of various hydrological variables, such as annual runoff (Arora, 2002; Jiang et al., 2017; Jiang et al., 2015; Liu et al., 2017; Xiong et al., 2014; Yang and Yang, 2013), flood (Chen et al., 2013; Gilroy and Mccuen, 2012; Gu et al., 2016; Kwon et al., 2008; López and Francés, 2013; Tang et al., 2015; Xiong et al., 2015b; Yan et al., 2016; Zhang et al., 2014; Zhang et al., 2015), low flow (Du et al., 2015; Jiang et al., 2014; Liu et al., 2015), precipitation (Cheng and AghaKouchak, 2014; Gu et al., 2017a, b, c; Mondal and Mujumdar, 2015; Villarini et al., 2010) and so on. Compared with the literatures on annual runoff, floods and precipitation, the literatures on the nonstationary analysis of low flow are relatively limited.

Previous hydrological literatures on frequency analysis of nonstationary hydrological series mainly focus on two aspects: development of nonstationary method and exploration of covariates reflecting changing environments. Strupczewski et al. (2001) presented the method of time-varying moment which assumes that the hydrological variable of interest obeys a certain distribution type, but its moments change over time. The method of time-varying moment was modified to be the method of time-varying parameter values for the distribution representative of hydrologic data (Richard et al., 2002). Villarini et al. (2009) presented this method using the Generalized Additive Models for Location, Scale, and Shape Parameters (GAMLSS) (Rigby and Stasinopoulos, 2005), a flexible framework to assess nonstationary time series. The time-varying parameter method can be extended to the physical covariate analysis by replacing time with any other physical covariates (Du et al., 2015; Jiang et al., 2014; Kwon et al., 2008; López and Francés, 2013; Liu et al., 2015; Villarini et al., 2010; Villarini and Strong, 2014). For example, Jiang et al. (2014) used reservoir index as an explanatory variable based on the time-varying copula method for bivariate frequency analysis of nonstationary low-flow series in Hanjiang River, China. Du et al. (2015) took precipitation and air temperature as the explanatory variables to explain the inter-annual variability in low flows of Weihe River, China. Liu et al. (2015) took Sea Surface Temperature in Nino3 region, the Pacific Decadal Oscillation, the sunspot number (3 years ahead), the winter areal temperature and precipitation as the candidate explanatory variables to explain the inter-annual variability in low flows of Yichang station, China. Kam and Sheffield (2015) ascribed the increasing inter-annual variability of low flows over the eastern United States to North Atlantic Oscillation and Pacific North America.

To our knowledge, compared with the nonstationary flood frequency analysis, the studies on the nonstationary frequency analysis of low-flow series is not very extensive because of incomplete knowledge of low flow generation (Smakhtin, 2001). Most of these studies explain nonstationarity of low-flow series only by using climatic indicators or a single indicator of human activity. However, the indicators of catchment conditions (e.g. recession rate) related to physical hydrological processes have seldom been attached in nonstationary modeling of low flow series.

This lack of linking with hydrological processes makes it impossible to accurately quantify the contributions of influencing factors for the nonstationarity of low flow series, and such a scientific demand for tracing the sources of nonstationarity of low-flow series and qualifying their contributions motivated the present study. The knowledge of low-flow generation has been increased by efforts of hydrologists, which can help develop physical covariates to address nonstationarity. Low flows generally originate from groundwater or other delayed outflows (Smakhtin, 2001; Tallaksen, 1995). Their generation relates to both an extended dry weather period (leading to a climatic water deficit) and complex hydrological processes which determine how these deficits propagate through the vegetation, soil and groundwater system to streamflow (WMO, 2009). Thus, not only climate condition drivers (e.g. potential evaporation exceeds precipitation), but also catchment condition drivers (e.g. the faster hydrologic response rate to precipitation) can cause low flows.

The significant factors such as precipitation, temperature, evapotranspiration, streamflow recession, large-scale teleconnections and human forces may play important roles in influencing low-flow generation (Botter et al., 2013; Giuntoli et al., 2013; Gottschalk et al., 2013; Jones et al., 2006; Kormos et al., 2016; Roderick et al., 2013; Sadri et al., 2015). Gottschalk et al. (2013) presented a derived low flow probability distribution function with climate and catchment characteristics parameters (i.e., the mean length of dry spells λ^{-1} and recession constant of streamflow K) as its distribution parameters. Botter et al. (2013) derived “a measurable index” (λ^{-1}/K) which can be used for discriminating erratic river flow regimes from persistent river flow regimes. Recently, Van Loon and Laaha (2015) used climate and catchment characteristics (e.g. the duration of dry spells in precipitation and the base flow index) to explain the duration and deficit of hydrological drought event and offered a further understanding of low-flow generation. These studies indicated that climate and catchment conditions play an important role in producing low flows.

The goal of this study is to trace origins of nonstationarity in low flows through developing a nonstationary low-flow frequency analysis framework with the consideration of the time-varying climate and catchment conditions (TCCCs) and human activity (HA). In this framework, the climate and catchment conditions are quantified using the eight indices, i.e., meteorological variables (total precipitation P, mean frequency of precipitation events λ, temperature T and potential evapotranspiration EP ~~ET~~), basin storage characteristics (base-flow index BFI , recession constant K) and aridity indexes (climate aridity index AI_{EP} ~~AI_{ET}~~ , the recession-related aridity index AI_K). The specific objectives of this study are: (1) to find the most important index to explain the nonstationarity of low-flow series; (2) to determine the best subset of TCCCs indices and/or human activity indices (i.e., population *POP*, irrigation area *IAR*, and gross domestic product *GDP*) for final model through stepwise selection method to identify nonstationary mode of low-flow series; and (3) to quantify the contribution of selected explanatory variables to the nonstationarity.

This paper is organized as follows. Section 2 describes the methods. The Weihe River basin and available data sets used in this study are described in Section 3, followed by a presentation of the results and discussion in Section 4. Section 5 summarizes the main conclusions.

2 Methodology

The flowchart of how to organize the nonstationary low-flow frequency analysis framework is shown in Fig. 1. The whole process is divided into three steps. The first step is preliminary analysis, including the graphical presentation of both explanatory variables and low-flow series, the statistical test for nonstationarity and the correlations between each explanatory variable and each low-flow series. The second step is single covariate analysis for the most important explanatory variable. The third step is multiple covariate analysis for the optimal combination. We use a low-flow frequency analysis model and stepwise regression method to accomplish the last two steps. In the following sub-sections, first, the low-flow frequency analysis model is constructed based on the nonstationary probability distributions method, in which distribution parameters serving as response variables can vary as functions of explanatory variables. Second, the distribution types used to build the nonstationary model are outlined. Then, the candidate explanatory variables related to the time-varying climate and catchment conditions (TCCCs) and human activity (HA) are clarified. Finally, estimation of model parameters and selection of models are illustrated.

<Figure 1>

2.1 Construction of the low-flow nonstationary frequency analysis model

Generally, a nonstationary frequency analysis model can be established based on the time-varying distribution parameters method (Du et al., 2015; López and Francés, 2013; Liu et al., 2015; Richard et al., 2002; Villarini and Strong, 2014). For the nonstationary probability distribution $f_Y\left(Y_t \middle| \boldsymbol{\theta}^t\right)$, let Y_t be a random variable at time t $(t=1,2,...,N)$ and vector $\boldsymbol{\theta}^t=[\theta_1^t,\theta_2^t,...,\theta_m^t]$ be the time-varying parameters. The number of parameters m in hydrological frequency analysis is generally limited to three or less. The function relationship between the k^{th} parameter θ_k^t and the multiple explanatory variables is expressed as follows:

$$g_k\left(\theta_k^t\right)=h_k\left(x_1^t,x_2^t,...,x_n^t\right) \tag{1}$$

where $x_1^t,x_2^t,...,x_n^t$ are explanatory variables; n is the number of explanatory variables; $g_k(\cdot)$ is the link function which ensures the compliance with restrictions on the sample space and is usually set to natural logarithm for the given negative predictions; $h_k(\cdot)$ is the function for nonstationary modeling. The theory of Generalized Linear Model (Dobson and Barnett, 2012) is used to build function relationships between distribution parameters and their explanatory variables. In GLMs, the response relationship can be generally expressed as

$$g_k\left(\theta_k^t\right)=\alpha_{0k}+\sum_{i=1}\alpha_{ik}x_i^t \tag{2}$$

where α_{ik} $(i=0,1,2,...,n,k=1,...,m)$ are the GLM parameters.

In order to compare the nonstationary models constructed by various combinations of explanatory variables, Eq. (2) is modified in this study using dimensionless method for the standard GLM parameters. The value of θ_k^t could be assumed to be equal to its mean ($\bar{\theta}_k$) when all explanatory variables are equal to their mean ($\bar{x}_i$), i.e.,

$$\theta_k^t\left(x_1^t=\bar{x}_1,x_2^t=\bar{x}_2,...,x_n^t=\bar{x}_n\right)=\bar{\theta}_k \tag{3}$$

Eq. (2) is then modified as

$$\begin{aligned}
&g_k\left(\frac{\theta_k^t}{\bar{\theta}_k}\right)=\beta_{0k}+\sum_{i=1}^{i=n}\beta_{ik}z_i^t\\
&z_i^t=\frac{x_i^t-\bar{x}_i}{s_i},\qquad i=1,2,\ldots,n\\
&\beta_{0k}=g_k\left(\frac{\theta_k^t}{\bar{\theta}_k}\middle|\theta_k^t=\bar{\theta}_k\right)=g_k\left(1\right)
\end{aligned} \tag{4}$$

where z_i^t is normalized explanatory variable; s_i is the standard deviation of x_i^t; β_{ik} $(i=1,2,...,n,k=1,...,m)$ are the standard GLM parameters. Let the link function $g_k(\cdot)$ be the natural logarithmic function $\ln(\cdot)$ and θ_l^t be the distribution parameter in $[\theta_1^t,\theta_2^t,...,\theta_m^t]$ with most significant change, the degree of nonstationarity in low flow series can be defined as $\ln(\theta_l^t)-\ln(\bar{\theta}_l)$. Then, the contribution c_i^t of each explanatory variable x_i^t to $\ln(\theta_l^t)-\ln(\bar{\theta}_l)$ could be defined as

$$c_i^t = \beta_{il} \frac{x_i^t - \overline{x}_i}{s_i} \tag{5}$$

2.2 Candidate distribution functions

We need to select the form of probability distribution $f_Y(\cdot)$ to determine what type of nonstationary frequency curves will be produced. Various probability distributions have been compared or suggested in modeling of low-flow series (Du et al., 2015; Hewa et al., 2007; Liu et al., 2015; Matalas, 1963; Smakhtin, 2001). An extensive overview of distribution functions for low flow is given in Tallaksen et al. (2004). Following these recommendations, we consider five distributions, i.e. Pearson-III (PIII), Gamma (GA), Weibull (WEI), Lognormal (LOGNO) and Generalized Extremes Value (GEV) as candidates in this study (Table 1). In the case of Pearson-III distribution, considering that the parameter θ_3 of Pearson-III as lower bound should approach zero and the parameter θ_3 of GEV is quite sensitive and difficult to be estimated, we assume them to be constant in this study.

2.3 Candidate explanatory variables

We look for variables $x_1^t, x_2^t, ..., x_n^t$ that can explain parts of the variations in distribution parameters $\boldsymbol{\theta}^t$. From the perspective of low-flow generation, the dependency between low-flow regime and both climate and catchment conditions has been presented by previous studies (Botter et al., 2013; Gottschalk et al., 2013; Van Loon and Laaha, 2015). We focus on eight measuring indices: total precipitation, mean frequency of precipitation events, temperature, potential evapotranspiration, climate aridity index, base-flow index, recession constant and recession-related aridity index. These indices were chosen to incorporate time-varying climate and catchment conditions (TCCCs) in nonstationary modeling of low-flow frequency and serving as candidate explanatory variables. The values of them at each year could be estimated from hydro-meteorological data. Annual precipitation (P) and temperature (T) are calculated directly by meteorological data. The remaining TCCCs indices need to be estimated indirectly. Detailed estimation procedures are shown in following subsections. In addition to TCCCs indices, the three indices of human activity (irrigation area, population and gross domestic product) are included, and the reasons for selecting all indices are summarized in Table 2.

2.3.1. Annual mean frequency of precipitation events (λ)

Annual mean frequency of precipitation events is defined as an index to represent the intensity of precipitation recharge to the streamflow:

$$\lambda = \frac{1}{W}\sum_{w=1}^{w=W}\frac{N_w\left(A\right)}{t_r} \tag{6}$$

where $N_w\left(A\right)$ is the number of daily rainfall events A (with values more than the threshold 0.5 mm) in w^{th} windows with a length t_r; W is the number of windows.

2.3.2. Annual climate aridity index (AI_{EP} ~~AI_{ET}~~)

The ratio of annual potential evaporation to precipitation, commonly known as the climate aridity index, has been used to assess the impacts of climate change on annual runoff (Arora, 2002; Jiang et al., 2015). The climate aridity index largely reflects the climatic regimes in a region and determines runoff rates (Arora, 2002). Therefore, we choose the annual climate aridity index as a measure of time-varying climate and catchment conditions and estimate its value in a whole region using

$$AI_{EP} = \frac{EP}{P} \cancel{AI_{ET} = \frac{ET}{P}} \tag{7}$$

where P is annual areal precipitation (mm); EP ~~ET~~ is annual areal potential evapotranspiration. The Hargreaves equation (Hargreaves and Samani, 1985) is applied to calculate EP ~~ET~~ using the R-package ‘Evapotranspiration’ (Guo, 2014).

2.3.3. Annual base-flow index (*BFI*)

The base flow index (*BFI*) is defined as the ratio of base flow to total flow. This index has been applied to quantify catchment conditions (e.g. soil, geology and storage-related descriptors) to explain hydrological drought severity (Van Loon and Laaha, 2015). We also choose annual base flow index (BFI) as a measure of TCCCs. BFI is estimated using a hydrograph separation procedure in R-package ‘lfstat’ (Koffler and Laaha, 2013).

2.3.4. Annual streamflow recession constant (*K*)

Recession constant is an important catchment characteristic index measuring the time scale of the hydrological response and reflecting water retention ability in the upstream catchment (Botter et al., 2013). Various estimation methods have been developed to extract recession segments and to parameterize characteristic recession behavior of a catchment (Hall, 1968; Sawaske and Freyberg, 2014; Tallaksen, 1995).

In this study, annual recession analysis (ARA) is performed to obtain annual streamflow recession constant (*K*). In ARA, the linearized Depuit-Boussinesq equation is used to parameterize characteristic recession behavior of a catchment and is written as

$$-\frac{dQ_t}{dt} = \frac{1}{K} Q_t \tag{8}$$

where Q_t is the value at time t. Eq. (8) is investigated by plotting data points $\frac{dQ_t}{dt}$ against Q_t of all extracted recession segments from hydrographs at each year. The criteria of recession segments extraction are based on the Manual on Low-flow Estimation and Prediction (WMO, 2009). Then, the annual recession rate (K^{-1}) is estimated as the slope of fitted straight line of these data points with least square method. We calculated K using R-package ‘lfstat’ (Koffler and Laaha, 2013).

2.3.5. Annual recession-related aridity index (AI_K)

In this study, recession-related aridity index is defined as the ratio of recession rate (K^{-1}) to mean precipitation frequency (λ), denoted as

$$AI_K = \frac{K^{-1}}{\lambda} \tag{9}$$

This ratio plays an important role in controlling river flow regime (Botter et al., 2013; Gottschalk et al., 2013) and serves as an indicator measuring the recession-related aridity degree of the streamflow in river channel. For example, faster recession process or lower precipitation frequency may lead to increased runoff loss or decreased precipitation supply. Consequently, the higher the value AI_K is, the more likely low flow events occur, and vice versa.

2.4 Parameter estimation

The model parameters including $\overline{\theta}_k (k=1,2,...,m)$ and β_{ik} $(i=1,2,...,n, k=1,...,m)$ are estimated. $\overline{\theta}_k (k=1,2,...,m)$ are estimated from outputs of stationary frequency analysis through maximum likelihood method. We have

$$L\left(\overline{\theta}_1, \overline{\theta}_2, ..., \overline{\theta}_m\right) = \sum_{t=1}^{t=N} \ln\left[f_Y\left(y_t \middle| \overline{\theta}_1, \overline{\theta}_2, ..., \overline{\theta}_m\right)\right] \tag{10}$$

where y_t is observed low flow at time t; N is the number of samples. The parameters β_{ik} $(i=1,2,...,n, k=1,...,m)$ are estimated through maximum likelihood method to produce nonstationary low-flow frequency curves:

$$L\begin{pmatrix}\beta_{11},...,\beta_{n1}\\ ...\\ \beta_{1m},...,\beta_{nm}\end{pmatrix}=\sum_{t=1}^{t=N}\ln\left\{f_Y\left(y_t\left|\theta_1^t\left(z_1^t,...,z_n^t\left|\beta_{11},...,\beta_{n1}\right.\right),...,\theta_m^t\left(z_1^t,...,z_n^t\left|\beta_{1m},...,\beta_{nm}\right.\right)\right.\right)\right\} \tag{11}$$

The residuals (normalized randomized quintile residuals) are used to test the goodness-of-fit of fitted model objects (Dunn and Symth, 1996):

$$\hat{r}_t=\Phi^{-1}\left(F_Y\left(y_t\left|\hat{\boldsymbol{\theta}}^t\right.\right)\right) \tag{12}$$

where $F_Y(\cdot)$ is the cumulative distribution of y_t; $\Phi^{-1}(\cdot)$ is the inverse function of the standard normal distribution. The distribution of the true residuals $\hat{r}_t$ converges to standard normal if the fitted model is correct. Worm plot (Buuren and Fredriks, 2001) is used to check whether $\hat{r}_t$ have a standard normal distribution.

2.5 Model selection

Model selection contains the selection of the type of probability distribution and the selection of the explanatory variables to explain the response variables (i.e., distribution parameters θ_1 and θ_2). In order to obtain the final optimal model, the selection of the explanatory variables for θ_1 and θ_2 is conducted by a stepwise selection strategies (Stasinopoulos and Rigby, 2007; Venables, 2002): i.e. select a best subset of candidate explanatory variables for θ_1 using a forward approach (which starts with no explanatory variable in the model and tests the addition of each explanatory variable using a chosen model fit criterion); given this subset for θ_1 select another subset for θ_2 (forward). The stepwise selection strategies can get a series of stepwise models with different numbers of explanatory variables, as shown in Fig1. In order to detect how the number of explanatory variables influences the performance of the model for describing non-stationarity, we investigate the eight types of stepwise models as shown in Table 3: the zero-covariate model or stationary model (M0), the time covariate model (M1), single physical covariate model M2 (single TCCCs covariate model M2a or single HA covariate model M2b), two TCCCs covariates model (M3), the optimal TCCCs covariates model (M4), the optimal HA covariates model (M5) and the final model (M6). The model fit criterion is based on the Akaike's information criterion (Akaike, 1974) as shown by the following

$$AIC = -2ML + 2df \tag{13}$$

where ML is the log-likelihood in Eq. (11) and df is the number of degrees of freedom. The model with the lower AIC value was considered better.

3. Study Area and Data

3.1. The study area

The Weihe River, located in the southeast of the Northwest Loess Plateau, is the largest tributary of the Yellow River, China. The Weihe River has a drainage area of 134 766 km^2, covering the coordinates of $33°42'$-$37°20'$N $104°18'$-$110°37'$E (Fig. 2). This catchment generally has a semi-arid climate, with extensive continental monsoonal influence. Average annual precipitation of the whole area over the period 1954-2009 is about 540 mm, and has a wide range

(400-1000 mm) in various regions. Under the significant impacts of climate change and human activities in the Weihe River basin in recent decades, the hydrological regime of the river has changed over time (Du et al., 2015; Jiang et al., 2015; Xiong et al., 2015a).

<Figure 2>

In the Weihe basin, the impacts of agricultural irrigation on runoff have been found to be significant (Jiang et al., 2015; Lin et al., 2012). Lin et al. (2012) mentioned that the annual runoff of the Weihe River was significantly affected by irrigation diversion of the Baoji Gorge irrigation area. The irrigated area of Baoji Gorge Irrigation Area increased over time since the founding of P.R. China in 1949, and due to one influential irrigation system project in that area, it became more than twice of the original irrigation area since 1971. Jiang et al. (2015) demonstrated that in the Weihe basin, irrigated area, as compared with the other indices e.g. population, gross domestic product and cultivated land area, was a more suitable human explanatory variable for explaining the time-varying behavior of annual runoff. With the above background, it is important to considering the effects of human activities that mainly originate from irrigation diversion, and especially for studying low flow series in this basin.~~ In this study, we use the available data (1980-2005) of the irrigation diversion system on plateau in Baoji Gorge Irrigation Area in Zhang (2008) to provide some information for the knowledge of low flow generation.~~ The estimations of annual recession rate (K^{-1}) by the daily streamflow data are expected to incorporate the information of impacts of water diversions on the low flows in the river channel.

3.2. Data

We used daily streamflow records (1954-2009) provided by the Hydrology Bureau of the Yellow River Conservancy Commission from both Huaxian station (with a drainage area of 106 500 km^2) and Xianyang station (with a drainage area of 46 480 km^2). Low-flow extreme events were selected from the daily streamflow series using the widely-used annual minimum series method (WMO, 2009). AM_n is the annual minimum *n*-day flow during hydrological year beginning on 1 March. Consequently, AM_1, AM_7, AM_{15} and AM_{30} are selected as low-flow extreme events in this study. The original measure unit of streamflow data ($\mathrm{m^3 \cdot s^{-1}}$) is converted to $10^{-4}\ \mathrm{m^3 \cdot s^{-1} \cdot km^{-2}}$ for convenience of comparison of results between the Huaxian and Xianyang gauging stations

We downloaded daily total precipitation and daily mean air temperature records for 19 meteorological stations over the basin from the National Climate Center of the China Meteorological Administration (source: http://cdc.cma.gov.cn). The areal average daily series of both variables above Huaxian and Xianyang stations are calculated using the Thiessen polygon method (Szolgayova et al., 2014; Thiessen, 1911). The annual average temperature (T) and annual total precipitation (P) over the period 1954-2009 are calculated for each catchment.

Human activity data (i.e. gross domestic product, population and irrigation area) were taken from annals of statistics provided by the Shaanxi Provincial Bureau of Statistics (http://www.shaanxitj.gov.cn/) and Gansu Provincial Bureau of Statistics (source: http://www.gstj.gov.cn/).

4. Results and discussion

4.1. Identification of nonstationarity

Graphical representation and statistical test provide a preliminary analysis for low-flow nonstationarity. The graphical representations of time-series data help visualize the trends of related variables (i.e. low-flow, TCCCs and HA variables), the density distributions of TCCCs variables and the correlations between low-flow variables and these explanatory variables. In Fig. 3, four annual minimum streamflow series (AM_1, AM_7, AM_{15} and AM_{30}) in both Huaxian and Xianyang gauging stations show overall decreasing trends, as indicated by the fitted (dashed) trend lines. Compared with Huaxian, Xianyang has a larger runoff modulus (the flow per square kilometer) and a larger decrease in annual minimum streamflow series. For example, the decline slope of AM_{30} is -0.0725 ($10^{-4}\,\mathrm{m}^3\cdot\mathrm{s}^{-1}\cdot\mathrm{km}^{-2}/\mathrm{yr}$) in Huaxian station while Xianyang station it is -0.1338 ($10^{-4}\,\mathrm{m}^3\cdot\mathrm{s}^{-1}\cdot\mathrm{km}^{-2}/\mathrm{yr}$).

<Figure 3>

Figure 4 shows the kernel density estimations and time processes of TCCCs variables for both Huaxian (H) and Xianyang (X) stations. The results show that these variables have different variation patterns. For example, the mean frequency of precipitation events (λ) has a decreasing trend, while temperature (T) has an increasing trend. As presented by Fig. 5, three HA variables have a significant upward trend, especially the irrigation area IAR which is increased greatly after about 1970, suggesting that the impact of human activities in this basin has increased over time.

<Figure 4>

<Figure 5>

The significance of trends in the four annual minimum streamflow series and TCCCs variables is tested by the Mann-Kendall trend test (Kendall, 1975; Mann, 1945; Yue et al., 2002), and the change points in these series are detected by the Pettitt's test (Pettitt, 1979). The results in Table 4 show that in both Huaxian and Xianyang stations, the decreasing trends in all the four low-flow series (AM_1, AM_7, AM_{15} and AM_{30}) and two explanatory variables (λ and P), and the increasing trends in T, ET, and AI_{EP} $\cancel{AI_{ET}}$ are significant at the 0.05 level (Table 4), but BFI shows no significant trends. However, K and AI_K had significantly decreasing trends only in Huaxian station ($p\text{-}value < 0.05$). The results of change-point detection show that all low-flow series are located at 1968-1971 ($p\text{-}value < 0.05$) except AM_{30} at Xianyang station whose change point is located at 1993 ($p\text{-}value < 0.05$); for the eight candidate explanatory variables, the change points of the variables related to temperature (T, EP $\cancel{ET}$, AI_{EP} $\cancel{AI_{ET}}$) in both stations are located at 1990-1993 ($p\text{-}value < 0.05$), the change points of the variables related to precipitation (λ, P) in both stations are close at 1984-1990 ($p\text{-}value \leq 0.186$) and the change points of the variables related to streamflow recession (K, AI_K) in Huaxian station are located at 1968-1971 ($p\text{-}value < 0.05$). However, BFI in both stations and K and AI_K in Xianyang station show no significant change points.

A preliminary attribution analysis is performed using the Pearson correlation matrix to investigate the relations between the annual minimum series and eight candidate explanatory variables. Figure 6 indicates that there are significant linear correlations between the four minimum low-flow series (AM_1, AM_7, AM_{15} and AM_{30}) and all the explanatory variables except GDP, have the absolute values of Pearson correlation coefficients larger than 0.27 ($p\text{-}value < 0.05$). These potential physical causes of nonstationarity in low flows are further considered by establishing low-flow nonstationary model with TCCCs and HA variables in the following section.

<Figure 6>

4.2. Nonstationary frequency analysis models

4.2.1 Single covariate models

Figure 7 presents the AIC values of the four types of models (M0, M1, M2a and M2b) fitted for the low flow series (AM_1, AM_7, AM_{15} and AM_{30}). Some interesting results are shown as follows. First, nonstationary models (M1, M2a and M2b) have lower AIC values than stationary model (M0), which suggests that nonstationary models are worth considering. Second, for Huaxian station, irrespective of the chosen explanatory variables, the distribution type plays an important role in modeling nonstationary low flow series. For example, PIII, GA and WEI distributions in AM_{15} and AM_{30} cases have lower AIC values than LOGNO and GEV distributions. However, for Xianyang, choosing a suitable explanatory variable may be more important than choosing a distribution type. For example, variables t, P, T, AI_{EP} ~~AI_{ET}~~, POP and IAR in most cases have lower AIC values than the other explanatory variables. Finally, in Huaxian, the lowest AIC values for modeling AM_1, AM_7, AM_{15} and AM_{30} are found in GEV_M2b_*IAR*, LOGNO_M2b_*IAR*, PIII_M2a_AI_K and GA_M2a_AI_K, respectively; while in Xianyang, the lowest AIC values for modeling AM_1, AM_7, AM_{15} and AM_{30} are found in GEV_M2b_*IAR*, GEV_M2b_*IAR*, PIII_M2b_*IAR* and GEV_M2b_*IAR*, respectively. These results indicated that for explaining nonstationarity of low flow in Huaxian station, IAR is the most dominant HA variable, and AI_K is the most dominant TCCCs variable; while in Xianyang, the most dominant HA variable is IAR, the most dominant TCCCs variables causing nonstationarity in AM_1, AM_7, AM_{15} and AM_{30} are K, AI_{EP} $\cancel{AI_{ET}}$, AI_{EP} $\cancel{AI_{ET}}$ and T, respectively.

<Figure 7>

Figure 8 shows the diagnostic assessment of the GA_M2 model (with the optimal explanatory variable) for AM_{30} in both Huaxian and Xianyang stations. The centile curve plots of GA_M2 (Figs. 8a and 8b) show the observed values of AM_{30}, the estimated median and the areas between the 5th and 95th centiles. Figure 8a shows the response relationship between AM_{30} and AI_K in Huaxian: the increase of AI_K means the smaller magnitude of low-flow events because a high value of AI_K (faster stream recession or fewer rainy days) may lead to faster water loss or less supply. In Fig. 8b, the higher values of IAR means the smaller magnitude of low flow events, which suggests that IAR plays an important role in driving low-flow generation in Xianyang. Figs 8c and 8d show that the worm points are within the 95% confidence intervals, thereby indicating a good model fit and a reasonable model construction.

<Figure 8>

4.2.2 Multiple covariate models

Figure 9 shows the AIC values of stationary model (M0), time covariate model (M1), physical covariate models (M2a, M2b, M3, M4, M5 and M6) for AM_{30}. As shown in Fig. 9, M4 (nonstationary GA distribution with the optimal TCCCs variables) has a good performance; after adding the HA variables, M6 with the lowest AIC value is attained; it can be found that the combination of multiple TCCCs variables plays a major role in changing the low flows of Weihe River, but the influence of HA variables shouldn't be ignored.

<Figure 9>

A summary of frequency analysis based on nonstationary GA distribution AM_{30} is presented in Table 5. We choose to focus on M4, M5 and M6. When only using TCCCs variables to model nonstationary low-flow frequency distribution, the results of M4 show the optimal combination of explanatory variables for all low-flow series contains more than three variables. For example, for AM_{30} of Huaxian, the optimal combination of TCCCs variables includes AI_K, BFI and AI_{EP} $\cancel{AI_{ET}}$. When only ~~using~~ HA variables are used, the results of M5 show IAR is important to the low flows in this area. And M4 has a better performance than M5. When using both TCCCs variables and HA variables, the results of M6 show the optimal combination contains multiple TCCCs variables and the irrigation area IAR. For Huaxian, the optimal combination of all explanatory variables is AI_K, IAR, BFI and AI_{EP}, while for Xianyang, the optimal combination is IAR, AI_{EP} $\cancel{AI_{ET}}$ and BFI. We can also find that if two TCCCs variables are highly correlated, they do not seem to be selected as the explanatory variables at the same time. For example, in terms of air temperature (T), evapotranspiration (EP $\cancel{ET}$) and the climate aridity index (AI_{EP} $\cancel{AI_{ET}}$), only one of them will appear in the optimal combination. This suggests that multicollinearity problem in multiple variables analysis can be reduced, which will help obtain more reliable GLMs parameters for contribution analysis.

The diagnostic assessment of the GA_M6 model for AM_{30} at two stations is presented by Fig. 10. The centile curve plots of GA_M6 (Figs. 10a and 10b) show the more sophisticated nonstationary modeling than GA_M2 (Fig 8). When using GA_M6 to model AM_{30} in Huaxian (Fig. 9a), similar to GA_M2, the lower low flows are found to also correspond to higher value of AI_K, but GA_M6 is able to identify the more complex variation patterns of low flows through the incorporation of IAR, BFI and AI_{EP}. Figures 10c and 10d show that the data points of worm plots of GA_M6 are almost within the 95% confidence intervals, thereby indicating an acceptable model fit and a reasonable model construction.

<Figure 10>

Figure 11 presents the contribution of each selected explanatory variable to $\ln\left(\theta_1^t\right)-\ln\left(\bar{\theta}_1\right)$ in observation year based on GA_M6 for AM_{30} in Huaxian and Xianyang. We can find that for Huaxian, the simulation value of $\ln\left(\theta_1^t\right)$ frequently occur below $\ln\left(\bar{\theta}_1\right)$ during the two periods of about 1970-1982 and 1993-2003, which is in accordance with the observed decrease in AM_{30} of Huaxian station during these periods. In the former period 1970-1982, both AI_K and BFI contribute a lot of negative amount to $\ln\left(\theta_1^t\right)-\ln\left(\bar{\theta}_1\right)$, whereas during 1993-2003, the contribution of both AI_K and BFI becomes much less. However, IAR has almost equal negative contribution to $\ln\left(\theta_1^t\right)-\ln\left(\overline{\theta}_1\right)$ in both periods. Unlike the former three variables, the significant negative contribution of AI_{EP} $\cancel{AI_{ET}}$ is only found in 1993-2003. For AM_{30} of Xianyang, the contribution of IAR, AI_{EP} $\cancel{AI_{ET}}$ and BFI is similar to that at Huaxian station in two periods, however AI_K is not included in the final model.

<Figure 11>

4.3. Discussion

The impacts of both human activities and climate change on low flows of the study area led to time-varying climate and catchment conditions (TCCCs). Nonstationary modeling for annual low flow series using TCCCs variables and/or HA variables as explanatory variables is clearly different from either the stationary model (M0) or the time covariate model (M1). The result demonstrates that considering multiple drivers (e.g. the variability in catchment conditions), especially in such an artificially influenced river, is necessary for nonstationary modeling of annual low flow series.

In this study area, nonstationary modeling considering TCCCs is supported by the following facts and findings. For human activities, an important milestone representative is the completion and operation of the irrigation system on plateau in Baoji Gorge Irrigation Area since 1971 (Sect. 3.1). Figure 5c shows the change of irrigation area in this basin. And the change-point detection test in Sect. 4.1 shows that significant change points of both annual recession constant (K) and low flow series occur exactly at around 1971. This result demonstrates that changes in both K and AM_{30} may involve a consequence of this project. In addition to human activities, climate change also makes a considerable contribution to nonstationarity of low flows, as suggested by nonstationary modeling using TCCCs variables with stepwise analysis. Actually, climate driving pattern may strengthen after nearly 1990, which is indicated by change-point detection test of both annual mean temperature (T) and annual precipitation (P) as well as the behavior of annual low flow series after nearly 1990. Therefore, the temporal variability in irrigation area, streamflow recession, air temperature and precipitation (the frequency and volume of rain events) should be the main driving factors of generating low flow regimes in this basin. Overall, the causes of nonstationarity in category for two gauging stations have no clear difference, but have some differences in the relative importance. As shown in Table 5, when modeling the low-flow series of Huaxian using TCCCs variables, the optimal model (M4) preferred the variables are related to recession process; however, for Xianyang, the preferred variables are related to temperature. The reason for this may be that as a downstream station, Huaxian station suffers more intensive human activity, so that the importance of temperature change to the low-flow change is reduced meanwhile the importance of streamflow recession (related to the capability of water storage) change is enhanced. Ignoring the negative impacts of the errors in estimating annual recession constant (K) which are caused by insufficient data points of extracted stream segments at some wet years may lead to the propagation of high errors in annual recession analysis, and accordingly affect the quality of nonstationary frequency analysis when ~~using~~ K is used as an explanatory variable. Further study will give more reliable estimation of K through improving annual recession analysis. Besides, it should be noted that the "population" recorded in the annals of statistics may not be equal to the actual population living in the catchment. If the “population” in the annals is used as explanatory variable, this difference may lead to uncertainty of model parameter estimations. Nonetheless, it is the best population data so far and the explanatory variable POP is excluded in the final model (M6).

The related researches (Jiang et al., 2015; Yang and Yang, 2011; Yang and Yang, 2013; Zhang et al., 2015) have applied the Budyko framework to analyze the impacts of climate change and/or human activity on annual runoff. Indeed, for annual runoff, the Budyko framework is a good method because it used the mean annual water-energy balance equation to consider generation process of total runoff. Unfortunately, to our knowledge, there is a lack of equation derived from basic physics laws for generation process of low flows. Therefore, we emphasize the importance of TCCCs variables to modeling of low-flow nonstationarity.

5. Conclusion

There is an increasing need to develop an effective nonstationary low-flow frequency model to deal with nonstationarities caused by climate change and time-varying anthropogenic activities. In this study, time-varying climate and catchment conditions (TCCCs) in the Weihe River basin were measured by annual time series of the eight indices, i.e., total precipitation (P), mean frequency of precipitation events (λ), temperature (T), potential evapotranspiration (EP $\cancel{ET}$), climate aridity index (AI_{EP} $\cancel{AI_{ET}}$), base-flow index (BFI), recession constant (K), and the recession-related aridity index (AI_K). The nonstationary distribution model was developed using both these eight TCCCs indices and/or there HA indices as candidate explanatory variables for frequency analysis of time-varying annual low flow series caused by multiple drivers. The main driving forces of the decrease in low flows in the Weihe River include reduced precipitation, warming climate, increasing irrigation area and faster streamflow recession. Therefore, a complex deterioration mechanism resulting from these factors demonstrates that in this arid and semi-arid area, the water resources could be vulnerable to adverse environmental changes, thus portending increasing water shortages. The nonstationary low-flow model considering TCCCs can provide the knowledge of low-flow generation mechanism and give more reliable design of low flows for infrastructure and water supply.

Acknowledgements

The study was financially supported by the National Natural Science Foundation of China (NSFC Grants 51525902 and 51479139), and projects from State Key Laboratory of Water Resources and Hydropower Engineering Science, Wuhan University. We greatly appreciate ~~two~~ three reviewers for their insightful comments and constructive suggestions that helped us to improve the manuscript.

Reference

Akaike, H.: A new look at the statistical model identification, IEEE Transactions on Automatic Control, 19, 716-723, 1974.

Arora, V. K.: The use of the aridity index to assess climate change effect on annual runoff, Journal of Hydrology, 265, 164-177, 2002.

Botter, G., Basso, S., Rodriguez-Iturbe, I., and Rinaldo, A.: Resilience of river flow regimes, Proc Natl Acad Sci U S A, 110, 12925-12930, 2013.

Bradford, M. J. and Heinonen, J. S.: Low Flows, Instream Flow Needs and Fish Ecology in Small Streams, Canadian Water Resources Journal, 33, 165-180, 2008.

Buuren, S. V. and Fredriks, M.: Worm plot: a simple diagnostic device for modelling growth reference curves, Statistics in Medicine, 20, 1259-1277, 2001.

Chen, X., Zhang, L., Xu, C.-Y., Zhang, J., and Ye, C.: Hydrological Design of Nonstationary Flood Extremes and Durations in Wujiang River, South China: Changing Properties, Causes, and Impacts, Mathematical Problems in Engineering,2013,(2013-6-2), 2013, 211-244, 2013.

Cheng, L. and AghaKouchak, A.: Nonstationary precipitation Intensity-Duration-Frequency curves for infrastructure design in a changing climate, Sci Rep, 4, 7093, 2014.

Dobson, A. J. and Barnett, A. G.: An Introduction to Generalized Linear Models, Third Edition, Journal of the Royal Statistical Society, 11, 272-272, 2012.

Du, T., Xiong, L., Xu, C.-Y., Gippel, C. J., Guo, S., and Liu, P.: Return period and risk analysis of nonstationary low-flow series under climate change, Journal of Hydrology, 527, 234-250, 2015.

Dunn, P. K. and Symth, G. K.: Randomized quantile residuals, Journal of Computational and Graphical Statistics, 5, 236-244, 1996.

Gilroy, K. L. and Mccuen, R. H.: A nonstationary flood frequency analysis method to adjust for future climate change and urbanization, Journal of Hydrology, s 414–415, 40-48, 2012.

Giuntoli, I., Renard, B., Vidal, J. P., and Bard, A.: Low flows in France and their relationship to large-scale climate indices, Journal of Hydrology, 482, 105-118, 2013.

Gottschalk, L., Yu, K.-x., Leblois, E., and Xiong, L.: Statistics of low flow: Theoretical derivation of the distribution of minimum streamflow series, Journal of Hydrology, 481, 204-219, 2013.

Gu, X., Zhang, Q., Singh, V. P., Chen, X., and Liu, L.: Nonstationarity in the occurrence rate of floods in the Tarim River basin, China, and related impacts of climate indices, Global & Planetary Change, 142, 1-13, 2016.

Gu, X., Zhang, Q., Singh, V. P., and Shi, P.: Changes in magnitude and frequency of heavy precipitation across China and its potential links to summer temperature, Journal of Hydrology, 547, 2017a.

Gu, X., Zhang, Q., Singh, V. P., and Shi, P.: Non-stationarities in the occurrence rate of heavy precipitation across China and its relationship to climate teleconnection patterns, International Journal of Climatology, 37, 4186-4198, 2017b.

Gu, X., Zhang, Q., Singh, V. P., and Shi, P.: Nonstationarity in timing of extreme precipitation across China and impact of tropical cyclones, Global & Planetary Change, 149, 153-165, 2017c.

Guo, D.: An R Package for Implementing Multiple Evapotranspiration Formulations, International Environmental Modelling and Software Society. 2014.

Hall, F. R.: Base flow recessions: A review, Water Resources Research, 4, 973-983, 1968.

Hargreaves, G. H. and Samani, Z. A.: Reference Crop Evapotranspiration From Temperature, 1, 96-99 1985.

Hewa, G. A., Wang, Q. J., McMahon, T. A., Nathan, R. J., and Peel, M. C.: Generalized extreme value distribution fitted by LH moments for low-flow frequency analysis, Water Resources Research, 43, 227-228, 2007.

Jiang, C., Xiong, L., Guo, S., Xia, J., and Xu, C.-Y.: A process-based insight into nonstationarity of the probability distribution of annual runoff, Water Resources Research, 2017.

Jiang, C., Xiong, L., Wang, D., Liu, P., Guo, S., and Xu, C.-Y.: Separating the impacts of climate change and human activities on runoff using the Budyko-type equations with time-varying parameters, Journal of Hydrology, 522, 326-338, 2015.

Jiang, C., Xiong, L., Xu, C.-Y., and Guo, S.: Bivariate frequency analysis of nonstationary low-flow series based on the time-varying copula, Hydrological Processes, 29, 1521-1534, 2015.

Jones, R. N., Chiew, F. H. S., Boughton, W. C., and Zhang, L.: Estimating the sensitivity of mean annual runoff to climate change using selected hydrological models, Advances in Water Resources, 29, 1419-1429, 2006.

Kam, J. and Sheffield, J.: Changes in the low flow regime over the eastern United States (1962–2011): variability, trends, and attributions, Climatic Change, 135, 639-653, 2015.

Kendall, M. G.: Rank Correlation Methods. , Griffin, Londom, 1975.

Koffler, D. and Laaha, G.: LFSTAT - Low-Flow Analysis in R, Egu General Assembly, 15, 2013.

Kormos, P. R., Luce, C. H., Wenger, S. J., and Berghuijs, W. R.: Trends and sensitivities of low streamflow extremes to discharge timing and magnitude in Pacific Northwest mountain streams, Water Resources Research, 52, 4990-5007, 2016.

Kwon, H.-H., Brown, C., and Lall, U.: Climate informed flood frequency analysis and prediction in Montana using hierarchical Bayesian modeling, Geophysical Research Letters, 35, L05404, 2008. López, J. and Francés, F.: Non-stationary flood frequency analysis in continental Spanish rivers, using climate and reservoir indices as external covariates, Hydrology and Earth System Sciences, 17, 3189-3203, 2013.

Lin, Q. C., Huai-En, L. I., and Xi-Jun, W. U.: Impact of Water Diversion of Baojixia Irrigation Area to the Weihe River Runoff, Yellow River, 34, 106-108, 2012.

Liu, D., Guo, S., Lian, Y., Xiong, L., and Chen, X.: Climate-informed low-flow frequency analysis using nonstationary modelling, Hydrological Processes, 29, 2112-2124, 2015.

Liu, J., Zhang, Q., Singh, V. P., and Shi, P.: Contribution of multiple climatic variables and human activities to streamflow changes across China, Journal of Hydrology, 545, 145–162 2017.

Mann, H. B.: Nonparametric Tests Against Trend, Econometrica, 13, 245-259, 1945.

Matalas, N. C.: Probability distribution of low flows, U.S. Geological Survey professional Paper, 434-A, 1963.

Milly, P. C. D., Betancourt, J., Falkenmark, M., Hirsch, R. M., Kundzewicz, Z. W., Lettenmaier, D. P., and Stouffer, R. J.: Stationarity Is Dead: Whither Water Management?, Science, 319, 573-574, 2008.

Mondal, A. and Mujumdar, P. P.: Modeling non-stationarity in intensity, duration and frequency of extreme rainfall over India, Journal of Hydrology, 521, 217-231, 2015.

Pettitt, A. N.: A Non-Parametric Approach to the Change-Point Problem, Journal of the Royal Statistical Society, 28, 126-135, 1979.

Richard, W. K., Marc, B. P., and Philippe, N.: Statistics of extremes in hydrology, Advances in Water Resources, 25, 1287-1304, 2002.

Rigby, R. A. and Stasinopoulos, D. M.: Generalized additive models for location, scale and shape, Appl. Statist., 54, 507-554, 2005.

Roderick, M. L., Sun, F., Lim, W. H., and Farquhar, G. D.: A general framework for understanding the response of the water cycle to global warming over land and ocean, Hydrology & Earth System Sciences Discussions, 10, 15263-15294, 2013.

Sadri, S., Kam, J., and Sheffield, J.: Nonstationarity of low flows and their timing in the eastern United States, Hydrology & Earth System Sciences Discussions, 12, 2761-2798, 2015.

Salas, J. D.: Analysis and modeling of hydrologic time series, Handbook of Hydrology, 1993.

Sawaske, S. R. and Freyberg, D. L.: An analysis of trends in baseflow recession and low-flows in rain-dominated coastal streams of the pacific coast, Journal of Hydrology, 519, 599-610, 2014.

Smakhtin, V. U.: Low flow hydrology： a review, Journal of Hydrology, 240, 147-186, 2001.

Stasinopoulos, D. M. and Rigby, R. A.: Generalized additive models for location scale and shape (GAMLSS) in R, Journal of Statistical Software, 23, 2007.

Strupczewski, W. G., Singh, V. P., and Feluch, W.: Non-stationary approach to at-site flood frequency modeling I. Maximum likelihood estimation, Journal of Hydrology, 248, 123-142, 2001.

Szolgayova, E., Parajka, J., Blöschl, G., and Bucher, C.: Long term variability of the Danube River flow and its relation to precipitation and air temperature, Journal of Hydrology, 519, 871-880, 2014.

Tallaksen, L. M.: A review of baseflow recession analysis, Journal of Hydrology, 165, 349-370, 1995.

Tallaksen, L. M., Madsen, H., and Hisdal, H.: Hydrological Drought- Processes and Estimation Methods for Streamflow and Groundwater, Elsevier B.V., the Netherlands, 2004.

Tang, Y., Xi, S., Chen, X., and Lian, Y.: Quantification of Multiple Climate Change and Human Activity Impact Factors on Flood Regimes in the Pearl River Delta of China, Advances in Meteorology, 2016, 1-11, 2015.

Thiessen, A. H.: Precipitation averages for large areas, Monthly Weather Review, 39, 1082-1084, 1911.

Van Loon, A. F. and Laaha, G.: Hydrological drought severity explained by climate and catchment characteristics, Journal of Hydrology, 526, 3-14, 2015.

Venables, W. N. a. R., B. D. (2002) Modern Applied Statistics with S. Fourth edition, 2002.

Villarini, G., Smith, J. A., and Napolitano, F.: Nonstationary modeling of a long record of rainfall and temperature over Rome, Advances in Water Resources, 33, 1256-1267, 2010.

Villarini, G., Smith, J. A., Serinaldi, F., Bales, J., Bates, P. D., and Krajewski, W. F.: Flood frequency analysis for nonstationary annual peak records in an urban drainage basin, Advances in Water Resources, 32, 1255-1266, 2009.

Villarini, G. and Strong, A.: Roles of climate and agricultural practices in discharge changes in an agricultural watershed in Iowa, Agriculture, Ecosystems & Environment, 188, 204-211, 2014.

WMO: Mannual on Low-fow Estimation and Prediction. WMO-No.1029, Switzerland, 2009.

Xiong, L., Du, T., Xu, C.-Y., Guo, S., Jiang, C., and Gippel, C. J.: Non-Stationary Annual Maximum Flood Frequency Analysis Using the Norming Constants Method to Consider Non-Stationarity in the Annual Daily Flow Series, Water Resources Management, 29, 3615-3633, 2015

Xiong, L., Jiang, C., and Du, T.: Statistical attribution analysis of the nonstationarity of the annual runoff series of the Weihe River, Water Science & Technology, 70, 939-946, 2014.

Yan, L., Xiong, L., Liu, D., Hu, T., and Xu, C.-Y.: Frequency analysis of nonstationary annual maximum flood series using the time‐varying two‐component mixture distributions, Hydrological Processes, 31, 69–89, 2017.

Yang, H. and Yang, D.: Derivation of climate elasticity of runoff to assess the effects of climate change on annual runoff, Water Resources Research, 47, 197-203, 2011.

Yang, H. and Yang, D.: Evaluating attribution of annual runoff change: according to climate elasticity derived using Budyko hypothesis, Egu General Assembly, 15, 14029, 2013.

Yu, K.-x., Xiong, L., and Gottschalk, L.: Derivation of low flow distribution functions using copulas, Journal of Hydrology, 508, 273-288, 2014.

Yue, S., Pilon, P., and Cavadias, G.: Power of the Mann–Kendall and Spearman's rho tests for detecting monotonic trends in hydrological series, Journal of Hydrology, 259, 254-271, 2002.

Zhang, Q., Gu, X., Singh, V. P., and Xiao, M.: Flood frequency analysis with consideration of hydrological alterations: Changing properties, causes and implications, Journal of Hydrology, 519, 803-813, 2014.

Zhang, Q., Gu, X., Singh, V. P., Xiao, M., and Chen, X.: Evaluation of flood frequency under non-stationarity resulting from climate indices and reservoir indices in the East River basin, China, Journal of Hydrology, 527, 565-575, 2015.

Zhang, S., Yang, H., Yang, D., and Jayawardena, A. W.: Quantifying the effect of vegetation change on the regional water balance within the Budyko framework, Geophysical Research Letters, 43, 1140-1148, 2015.

~~Zhang, Y. P.: Economical water-use mode research of Baoji Gorge Irrigation Area based on WebGIS. Chinese, 2008.~~

Figure

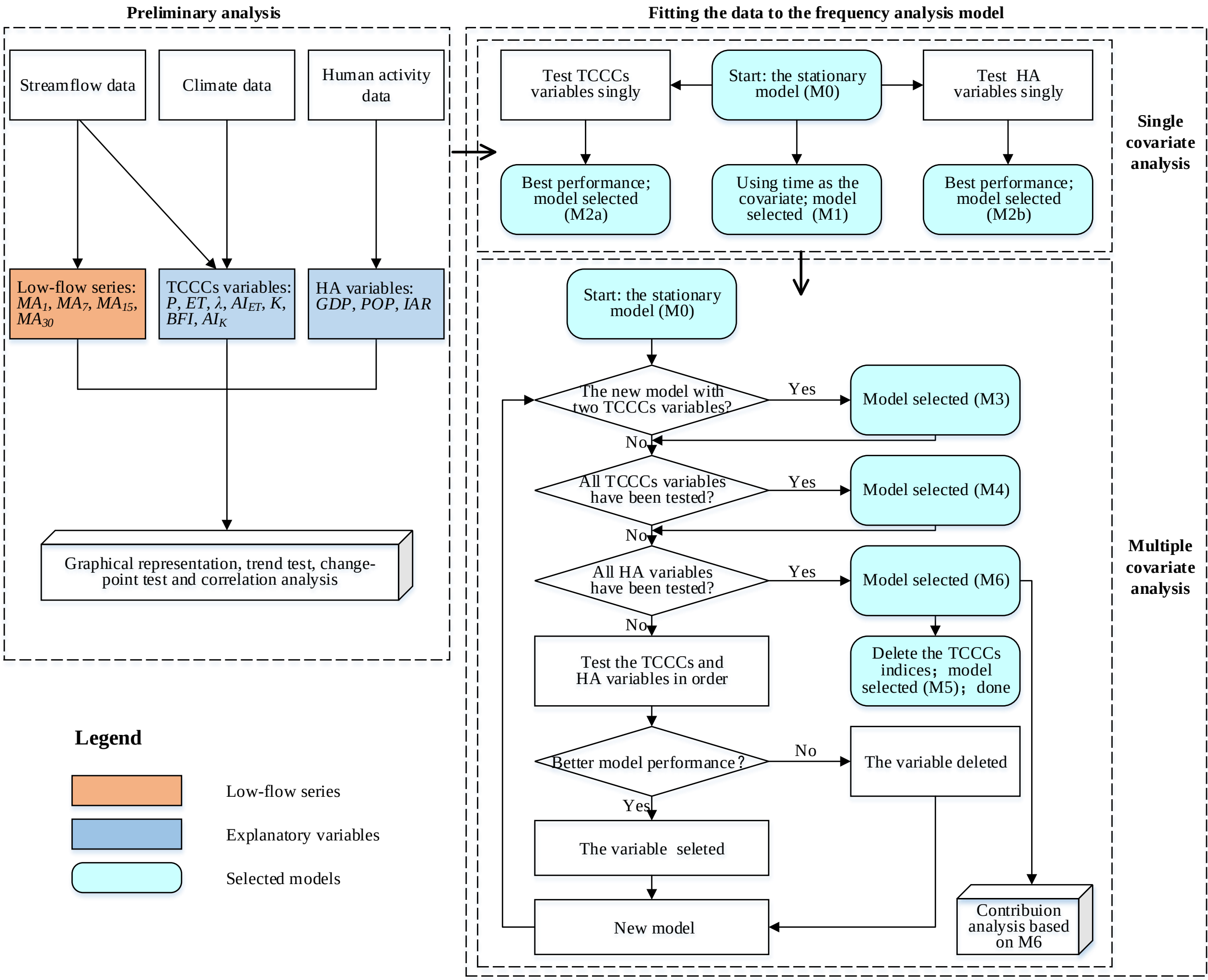

Figure 1. The framework of nonstationary low-flow frequency analysis.

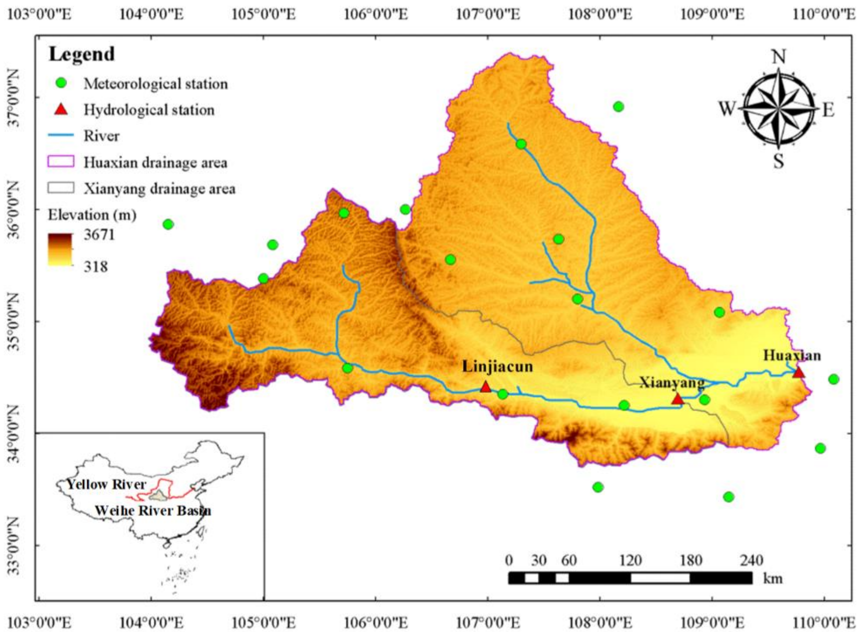

Figure 2. Location, topography, hydro-meteorological stations and river systems of the Weihe River basin.

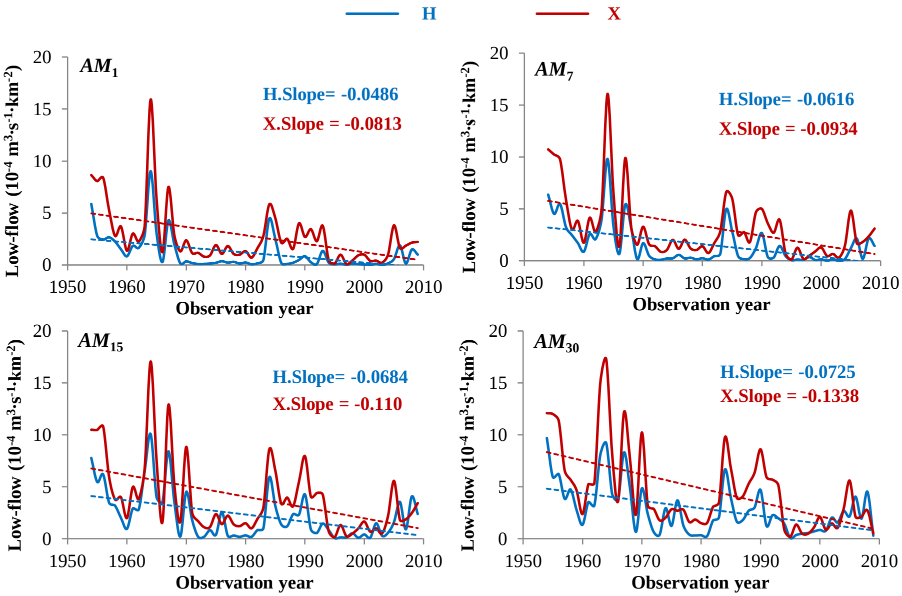

Figure 3. The annual minimum low flows and fitted trend lines in both Huaxian (H) and Xianyang (X) gauging stations.

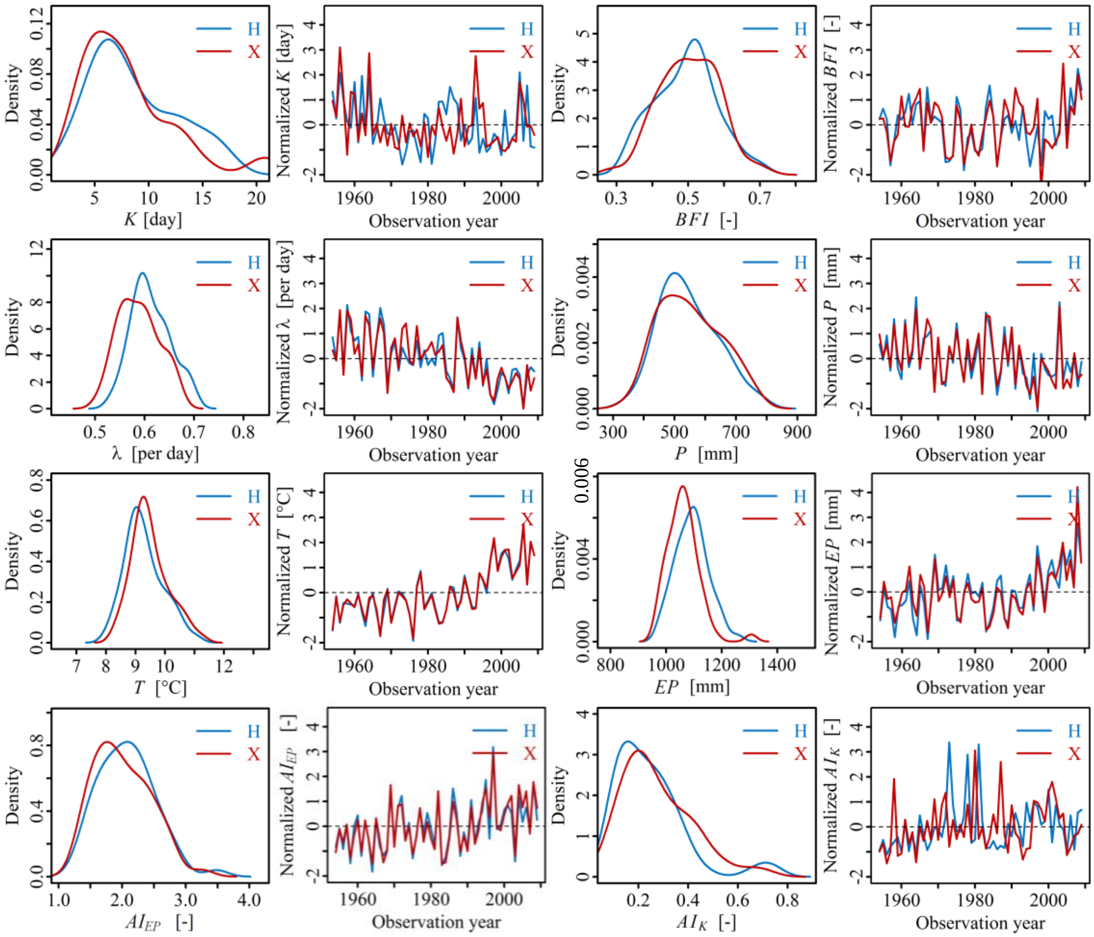

Figure 4. Frequency distributions (using the kernel density estimations) and time series processes of TCCCs variables in both Huaxian (H) and Xianyang (X) stations.

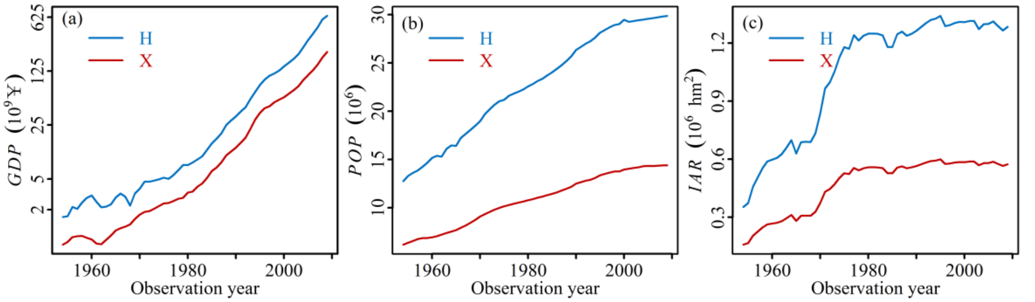

Figure 5. HA indices in both Huaxian (H) and Xianyang (X). (a), (b) and (c) are for population (*POP*), gross domestic production (*GDP*) and irrigated area (*IAR*), respectively.

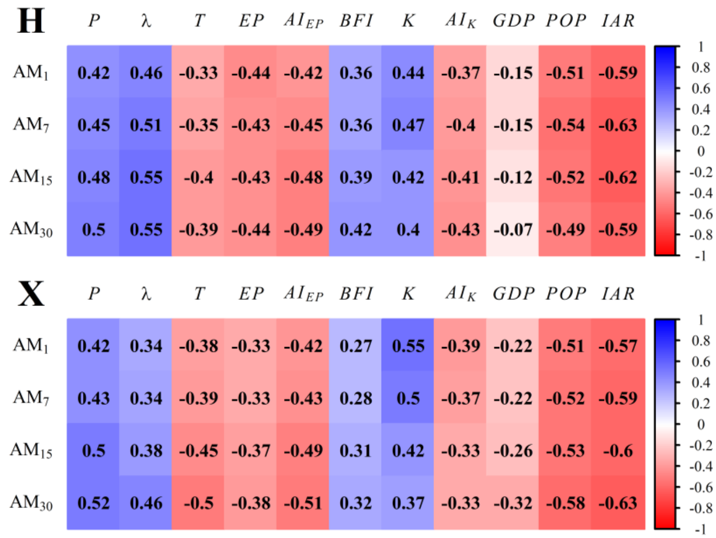

Figure 6. The Pearson correlation coefficients matrix between the annual minimum flow series and candidate explanatory variables in Huaxian (H) and Xianyang (X) stations; the darker color intensity represents a higher level of correlation (blue indicates positive correlation, and red indicates negative correlations).

H

AM_1	LOGNO	PIII	GEV	WEI	GA	AIC
M0_none	112.4	112.9	114.3	108.6	110.9	114.3
M1_*t*	94.8	97.0	90.3	94.4	97.0	
M2a_*P*	106.9	97.9	104.5	97.2	97.9	
M2a_*λ*	99.9	99.1	97.8	96.9	99.1	
M2a_*T*	101.6	102.8	99.9	100.5	102.8	
M2a_*EP*	101.5	99.9	100.5	98.3	99.9	
M2a_AI_{EP}	104.8	96.8	103.0	95.8	96.8	
M2a_*BFI*	103.4	99.2	97.6	96.7	99.2	
M2a_*K*	102.5	96.7	101.5	95.4	96.7	
M2a_AI_K	103.6	95.8	101.8	95.0	95.8	
M2b_*GDP*	109.5	107.6	105.7	105.8	107.6	
M2b_*POP*	91.9	94.5	85.2	91.6	94.5	
M2b_*IAR*	90.3	91.5	83.8	88.1	91.5	83.8

OPTIPAL MODEL: GEV_M2b_*IAR*

AM_7	LOGNO	PIII	GEV	WEI	GA	AIC
M0_none	151.8	155.0	158.2	153.5	155.2	158.2
M1_*t*	134.7	138.5	137.9	139.1	140.7	
M2a_*P*	144.6	138.5	147.4	140.4	140.7	
M2a_*λ*	137.7	139.4	142.4	140.3	141.6	
M2a_*T*	141.6	144.6	144.4	145.2	146.7	
M2a_*EP*	141.6	142.6	147.0	143.7	144.8	
M2a_AI_{EP}	142.7	137.9	146.2	139.5	140.0	
M2a_*BFI*	141.8	141.5	146.1	142.1	143.7	
M2a_*K*	139.9	138.3	146.3	139.7	140.5	
M2a_AI_K	139.9	135.7	140.7	137.7	138.0	
M2b_*GDP*	149.0	149.7	151.7	150.6	151.9	
M2b_*POP*	131.7	136.0	134.0	136.5	138.2	
M2b_*IAR*	127.9	132.3	130.7	132.5	134.5	127.9

OPTIPAL MODEL: LOGNO_M2b_*IAR*

AM_{15}	LOGNO	PIII	GEV	WEI	GA	AIC
M0_none	211.9	203.6	222.2	209.0	209.0	222.2
M1_*t*	200.6	190.2	210.1	197.5	197.4	
M2a_*P*	200.6	187.6	210.3	195.0	194.9	
M2a_*λ*	197.6	188.3	204.7	195.4	195.4	
M2a_*T*	201.8	193.5	209.0	200.7	200.8	
M2a_*EP*	202.3	192.7	210.6	199.9	199.9	
M2a_AI_{EP}	199.4	187.3	209.0	194.6	194.5	
M2a_*BFI*	200.7	190.4	209.3	197.7	197.7	
M2a_*K*	199.9	190.7	208.0	198.0	198.0	
M2a_AI_K	197.5	184.2	205.7	192.3	192.2	
M2b_*GDP*	209.8	199.0	220.2	206.5	206.5	
M2b_*POP*	197.7	188.0	206.5	195.1	195.1	
M2b_*IAR*	192.8	184.2	200.2	191.1	191.2	184.2

OPTIPAL MODEL: PIII_M2b_AI_K

AM_{30}	LOGNO	PIII	GEV	WEI	GA	AIC
M0_none	241.4	237.3	244.1	236.5	236.3	244.1
M1_*t*	233.0	225.4	233.5	225.4	225.5	
M2a_*P*	229.0	220.9	228.4	220.6	220.6	
M2a_*λ*	228.5	221.4	227.1	221.1	221.1	
M2a_*T*	233.4	227.2	232.2	227.7	227.5	
M2a_*EP*	232.9	226.2	233.3	226.4	226.4	
M2a_AI_{EP}	228.1	220.5	227.5	220.1	220.1	
M2a_*BFI*	226.2	223.5	228.5	224.0	223.5	
M2a_*K*	230.1	224.9	232.6	225.1	225.0	
M2a_AI_K	224.5	217.5	220.8	217.7	217.4	
M2b_*GDP*	239.3	233.1	236.1	234.2	234.1	
M2b_*POP*	230.4	223.1	230.2	223.0	223.0	
M2b_*IAR*	224.4	218.9	222.8	218.6	218.3	217.4

OPTIPAL MODEL: GA_M2b_AI_K

X

AM_1	LOGNO	PIII	GEV	WEI	GA	AIC
M0_none	227.2	226.5	228.0	227.2	226.3	228.0
M1_*t*	211.1	210.6	209.5	211.5	209.9	
M2a_*P*	215.6	211.9	215.6	212.9	211.5	
M2a_*λ*	217.2	216.1	218.6	217.7	216.5	
M2a_*T*	211.9	212.8	211.5	214.4	212.7	
M2a_*EP*	217.0	216.6	214.9	218.4	217.1	
M2a_AI_{EP}	213.6	211.3	214.1	212.3	210.8	
M2a_*BFI*	220.8	217.0	218.8	218.9	217.7	
M2a_*K*	215.4	211.4	212.9	212.2	210.7	
M2a_AI_K	218.2	214.0	217.4	215.2	214.0	
M2b_*GDP*	222.5	220.0	219.3	221.7	220.7	
M2b_*POP*	208.8	207.6	207.4	209.7	207.8	
M2b_*IAR*	208.0	206.1	205.1	208.2	206.3	205.1

OPTIPAL MODEL: GEV_M2b_*IAR*

AM_7	LOGNO	PIII	GEV	WEI	GA	AIC
M0_none	243.5	243.8	245.8	245.1	244.1	245.8
M1_*t*	227.9	228.2	228.0	229.7	227.9	
M2a_*P*	232.3	229.0	233.6	230.4	229.0	
M2a_*λ*	233.8	233.3	236.8	235.5	234.2	
M2a_*T*	229.1	230.1	230.5	232.2	230.3	
M2a_*EP*	234.4	234.0	234.7	236.4	235.0	
M2a_AI_{EP}	230.6	228.5	232.6	230.0	228.4	
M2a_*BFI*	235.9	234.2	236.2	236.8	235.4	
M2a_*K*	233.1	230.6	232.5	232.3	230.7	
M2a_AI_K	235.6	232.2	236.3	234.1	232.8	
M2b_*GDP*	239.1	237.7	238.7	239.8	238.7	
M2b_*POP*	225.5	225.5	225.8	227.9	226.0	
M2b_*IAR*	223.5	223.2	222.5	225.7	223.6	222.5

OPTIPAL MODEL:GEV_ M2b_*IAR*

AM_{15}	LOGNO	PIII	GEV	WEI	GA	AIC
M0_none	269.9	269.3	273.3	270.0	269.3	273.3
M1_*t*	254.5	253.5	256.1	254.6	253.4	
M2a_*P*	256.2	251.6	258.9	252.4	251.4	
M2a_*λ*	259.3	257.4	263.4	259.0	258.1	
M2a_*T*	254.3	253.5	256.7	255.0	253.6	
M2a_*EP*	260.6	258.5	262.7	260.2	259.3	
M2a_AI_{EP}	254.7	251.3	258.2	252.1	251.0	
M2a_*BFI*	261.6	258.6	262.7	260.5	259.5	
M2a_*K*	262.0	259.0	262.9	260.8	259.8	
M2a_AI_K	263.1	259.2	264.8	261.0	260.2	
M2b_*GDP*	265.0	262.1	266.9	263.7	263.0	
M2b_*POP*	252.3	251.4	253.8	253.2	251.9	
M2b_*IAR*	250.3	249.5	250.5	251.4	249.9	249.5

OPTIPAL MODEL:PIII_ M2b_*IAR*

AM_{30}	LOGNO	PIII	GEV	WEI	GA	AIC
M0_none	290.7	290.6	293.4	290.8	289.8	293.4
M1_*t*	271.6	270.4	271.5	271.8	270.1	
M2a_*P*	275.1	271.1	277.0	272.1	270.9	
M2a_*λ*	276.9	274.7	279.6	276.0	274.8	
M2a_*T*	270.8	270.3	271.1	272.1	270.1	
M2a_*EP*	280.9	278.3	282.1	279.9	278.7	
M2a_AI_{EP}	273.7	270.5	276.0	271.6	270.2	
M2a_*BFI*	282.3	278.8	284.1	280.3	279.3	
M2a_*K*	284.0	281.1	284.1	282.9	281.7	
M2a_AI_K	283.9	279.9	284.0	281.5	280.5	
M2b_*GDP*	283.3	279.5	283.5	281.0	280.1	
M2b_*POP*	269.4	268.5	269.3	270.5	268.6	
M2b_*IAR*	268.4	267.8	267.2	269.9	267.8	267.2

OPTIPAL MODEL: GEV_M2b_*IAR*

Figure 7. Comparisons among M0, M1 and M2 based on the AIC values for the four observed low-flow series in Huaxian (H) at left panel and Xianyang (X) at right panel; darker red color represents a higher goodness of fit.

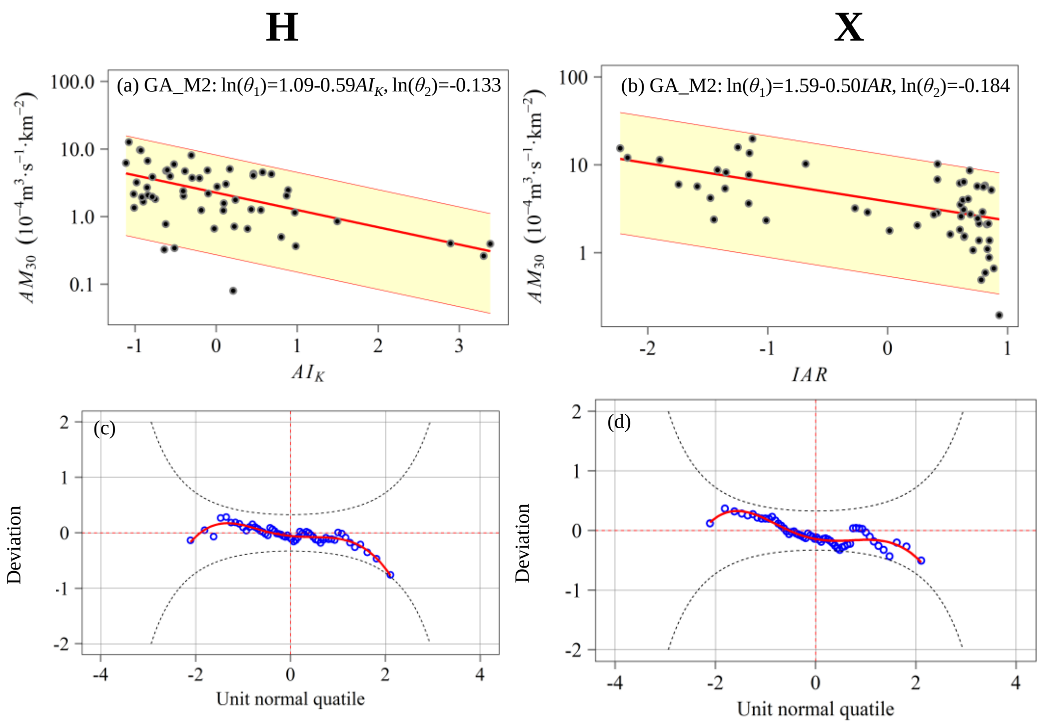

Figure 8. Performance assessments of GA_M2 for AM_{30} in Huaxian (H) at left panel and Xianyang (X) at right panel. (a) and (b) are the centile curves plots of GA_M2 (red lines represent the centile curves estimated by GA_M2; the 50th centile curves are indicated by thick red; the yellow-filled areas are between the 5th and 95th centile curves; the black points indicate the observed series); (c) and (d) are the worm plots of GA_M2 for the goodness-of-fit test; a reasonable model fit should have the data points fall within the 95% confidence intervals (between the two red dashed curves).

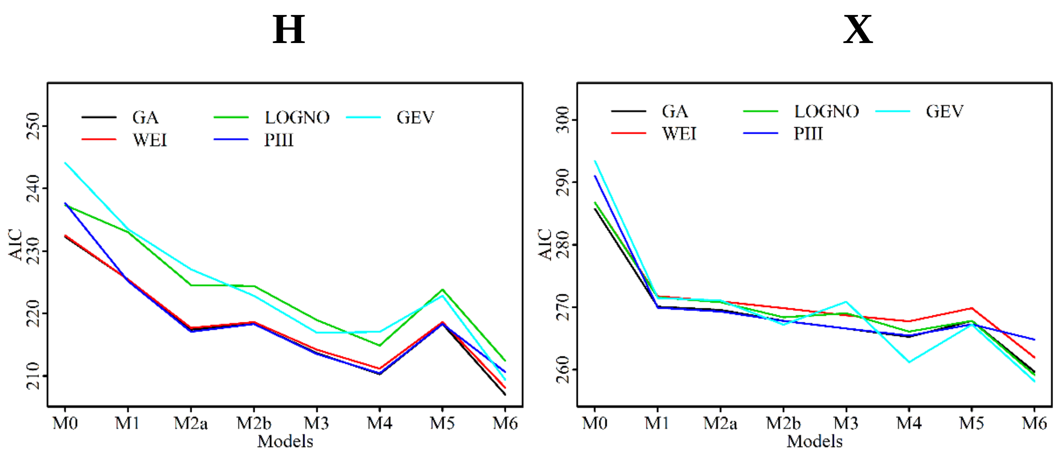

Figure 9. Comparisons of performance of stationary model (M0), time covariate model (M1) and physical covariate models (M2a, M2b, M3, M4, M5 and M6 with their corresponding optimal explanatory variables) for AM_{30} in Huaxian (H) at left panel and Xianyang (X) at right panel.

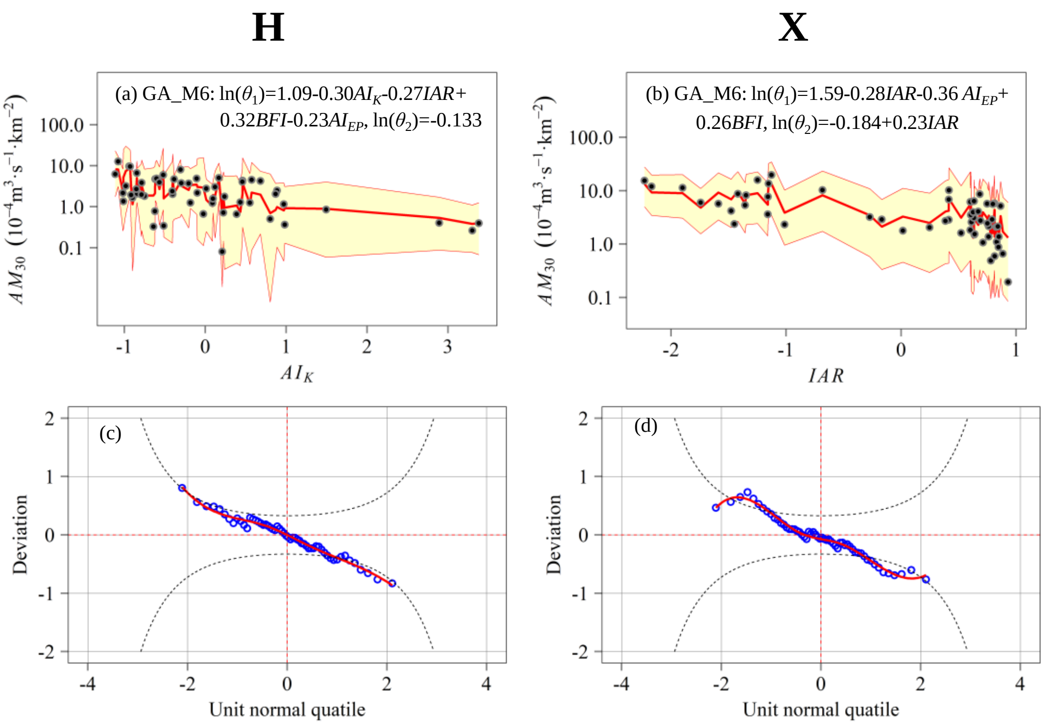

Figure 10. Performance assessments of GA_M6 for AM_{30} in Huaxian (H) at left panel and Xianyang (X) at right panel. (a) and (b) are the centile curves plots of GA_M6 (red lines represent the centile curves estimated by GA_M6; the 50th centile curves are indicated by thick red; the yellow-filled areas are between the 5th and 95th centile curves; the filled black points indicate the observed series); (c) and (d) are the worm plots of GA_M6 for the goodness-of-fit test; A reasonable model fit should have the data points fall within the 95% confidence intervals (between the two red dashed curves).

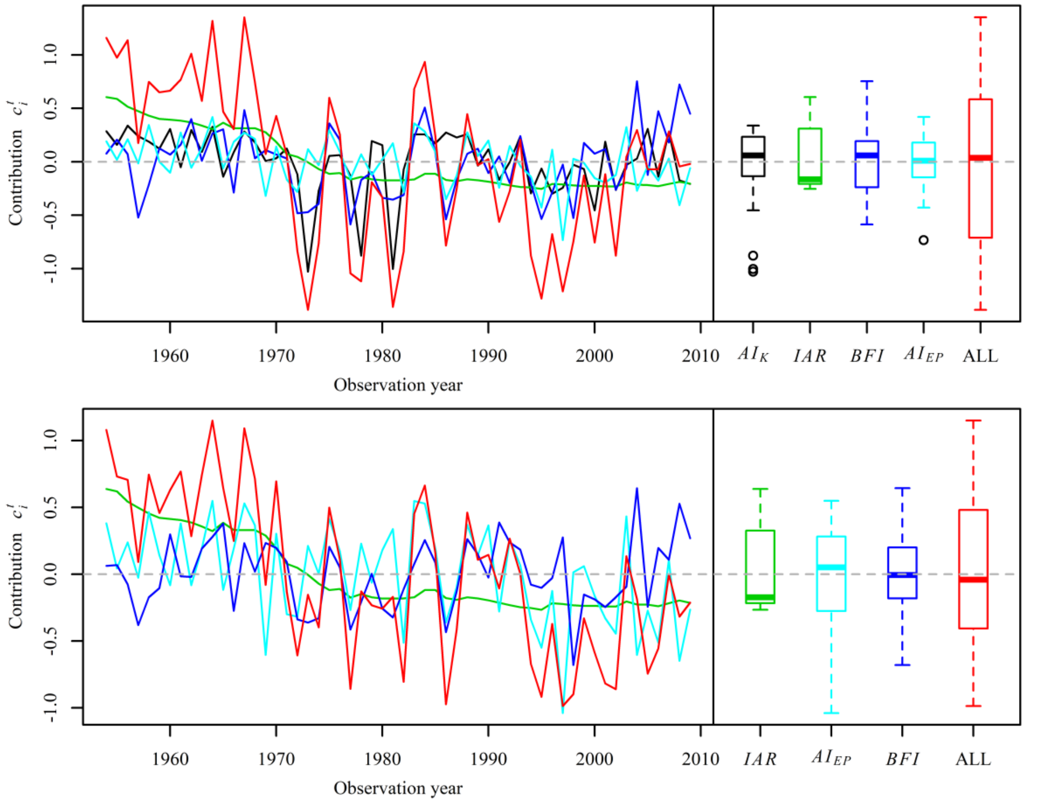

Figure 11. Contribution of selected explanatory variables to $c_i^t = \ln\left(\theta_1^t\right) - \ln\left(\overline{\theta}_1\right)$ in different periods based on GA_M6.

Table

Table 1. The probability density functions and moments (the mean and variance) for the candidate distributions in this study.

Distributions	Probability density function	Distribution moments
Pearson-III	$f_Y\left(y\|\theta_1,\theta_2,\theta_3\right)=\frac{\left(y-\theta_3\right)^{1/\theta_2^2-1}}{\Gamma\left(1/\theta_2^2\right)\left(\theta_1\theta_2^2\right)^{1/\theta_2^2}}\exp\left(-\frac{y-\theta_3}{\theta_1\theta_2^2}\right)$ $y>\theta_3,\theta_3>0,\theta_1>0,\theta_2>0$	$E[Y]=\theta_1+\theta_3$ $Var[Y]=\theta_1^2\theta_2^2$
Gamma	$f_Y\left(y\|\theta_1,\theta_2\right)=\frac{\left(y\right)^{1/\theta_2^2-1}}{\Gamma\left(1/\theta_2^2\right)\left(\theta_1\theta_2^2\right)^{1/\theta_2^2}}\exp\left(-\frac{y}{\theta_1\theta_2^2}\right)$ $y>0,\theta_1>0,\theta_2>0$	$E[Y]=\theta_1$ $Var[Y]=\theta_1^2\theta_2^2$
Weibull	$f_Y\left(y\|\theta_1,\theta_2\right)=\left(\frac{\theta_2}{\theta_1}\right)\left(\frac{y}{\theta_1}\right)^{\theta_2-1}\exp\left(-\left(\frac{y}{\theta_1}\right)^{\theta_2}\right)$ $y>0,\theta_1>0,\theta_2>0$	$E[Y]=\theta_1\Gamma\left(1+1/\theta_2\right)$ $Var[Y]=\theta_1^2\left[\Gamma\left(1+\frac{2}{\theta_2}\right)-\Gamma^2\left(1+\frac{1}{\theta_2}\right)\right]$
Lognormal	$f_Y\left(y\|\theta_1,\theta_2\right)=\frac{1}{y\theta_2\sqrt{2\pi}}\exp\left\{-\frac{\left[\log\left(y\right)-\theta_1\right]^2}{2\theta_2^2}\right\}$ $y>0,\theta_2>0$	$E[Y]=w^{1/2}e^{\theta_1}$ $Var[Y]=w\left(w-1\right)e^{2\theta_1}$ $w=\exp\left(\theta_2^2\right)$
GEV	$f_Y\left(y\|\theta_1,\theta_2,\theta_3\right)=\frac{1}{\theta_2}\left[1+\theta_3\left(\frac{y-\theta_1}{\theta_2}\right)\right]^{-1/\theta_3-1}\exp\left\{-\left[1+\theta_3\left(\frac{y-\theta_1}{\theta_2}\right)\right]^{-1/\theta_3}\right\}$ $-\infty<\theta_1<\infty,\theta_2>0,-\infty<\theta_3<\infty$	$E[Y]=\theta_1-\frac{\theta_2}{\theta_3}+\frac{\theta_2}{\theta_3}\eta_1$ $Var[Y]=\theta_2^2\left(\eta_2-\eta_1^2\right)/\theta_3^2$ $\eta_m=\Gamma\left(1-m\theta_3\right)$

Table 2. Description of the developed nonstationary models using time, TCCCs indices and/or HA indices as explanatory variables.

Model codes	Distribution					Description	
	GA	WEI	LOGNO	PIII	GEV	Variable category	The numbers of variables
M0	GA_M0	WEI_M0	LOGNO_M0	PIII_M0	GEV_M0	-	Zero
M1	GA_M1	WEI_M1	LOGNO_M1	PIII_M1	GEV_M1	Time	One
M2a	GA_M2a	WEI_M2a	LOGNO_M2a	PIII_M2a	GEV_M2a	TCCCs	One
M2b	GA_M2b	WEI_M2b	LOGNO_M2b	PIII_M2b	GEV_M2b	HA	One
M3	GA_M3	WEI_M3	LOGNO_M3	PIII_M3	GEV_M3	TCCCs	Two
M4	GA_M4	WEI_M4	LOGNO_M4	PIII_M4	GEV_M4	TCCCs	Identified by the stepwise selection
M5	GA_M5	WEI_M5	LOGNO_M5	PIII_M5	GEV_M5	HA	Identified by the stepwise selection
M6	GA_M6	WEI_M6	LOGNO_M6	PIII_M6	GEV_M6	TCCCs+HA	Identified by the stepwise selection

Table 3. The summary of candidate explanatory variables and reason of selection.

Category	Name	Indices	Reason of selection (related to)	Unit
TCCCs				
	P	Precipitation	Main supply source	mm
	λ	Mean frequency of precipitation events	Water supply intensity	per day
	T	Temperature	Evaporation loss	℃
	EP~~ET~~	Potential evapotranspiration	Evaporation loss	mm
	AI_{EP}~~AI_{ET}~~	Climate aridity index	Degree of meteorological drought	-
	BFI	Base-flow index	Water storage capability	-
	K	Recession constant	Water storage capability	day
	AI_K	Recession-related aridity index	Both the water storage and supply capability	-
HA				
	IAR	Irrigation area	Both irrigation diversion and evaporation loss	10^6 hm^2
	POP	Population	Water withdrawal loss for agricultural, domestic and industrial purposes	10^6
	GDP	Gross domestic product	Water withdrawal loss for agricultural, domestic and industrial purposes	10^9 ￥

Table 4. The results of trend test and change-point detection for both the four low flow series and TCCCs variables in Huaxian and Xianyang.

Station	Variable	Mann-Kendall test		Pettitt's test	
		S	*p-value*	Change point	*p-value*
Huaxian					
	AM_1	-564	6.91E-05(***)	1968	1.34E-03(**)
	AM_7	-560	7.79E-05(***)	1968	1.44E-03(**)
	AM_{15}	-438	2.01E-03(**)	1971	4.85E-03(**)
	AM_{30}	-378	7.71E-03(**)	1971	9.96E-03(**)
	P	-292	3.97E-02(*)	1985	1.86E-01( )
	λ	-632	8.20E-06(***)	1984	3.02E-04(***)
	T	752	1.11E-07(***)	1993	8.17E-06(***)
	EP~~ET~~	548	1.11E-04(***)	1993	1.98E-03(**)
	AI_{EP}~~AI_{ET}~~	384	6.79E-03(**)	1990	6.03E-02(.)
	BFI	52	7.19E-01( )	1998	3.88E-01( )
	K	-312	2.79E-02(*)	1968	8.11E-02(.)
	AI_K	376	8.04E-03(**)	1971	3.60E-02(*)
Xianyang					
	AM_1	-517	2.65E-04(***)	1968	2.2E-03(**)
	AM_7	-483	6.58E-04(***)	1970	2.5E-03(**)
	AM_{15}	-474	8.29E-04(***)	1971	2.2E-03(**)
	AM_{30}	-570	5.78E-05(***)	1993	4.5E-04(***)
	P	-414	3.51E-03(**)	1990	1.45E-02(*)
	λ	-652	4.21E-06(***)	1984	6.00E-05(***)
	T	724	3.22E-07(***)	1993	5.41E-06(***)
	EP~~ET~~	372	8.74E-03(**)	1993	3.01E-03(**)
	AI_{EP}~~AI_{ET}~~	454	1.37E-03(**)	1993	8.82E-03(**)
	BFI	64	6.56E-01( )	2003	8.65E-01( )
	K	-210	1.39E-01( )	1966	2.03E-01( )
	AI_K	290	4.11E-02(*)	1968	1.63E-01( )

Signif. codes: 0 '***' 0.001 '**' 0.01 '*' 0.05 '.' 0.1 ' ' 1

Table 5. The summary of frequency analysis using GA distribution for AM_{30} in Huaxian and Xianyang.

Station	Model codes	Optimal variable	AIC	Distribution parameters		
				$\ln(\theta_1)$	$\ln(\theta_2)$	θ_3
Huaxian						
	GA_M0	-	232.3	1.09	-0.133	-
	GA_M1	t	225.5	1.09-0.32t	-0.133	-
	GA_M2	AI_K	217.4	1.09-0.59AI_K	-0.133	-
	GA_M2b	IAR	218.3	1.09-0.47IAR	-0.133	-
	GA_M3	AI_K, BFI	213.7	1.09-0.50AI_K +0.32BFI	-0.133	-
	GA_M4	AI_K, BFI, $AI_{EP}\cancel{AI_{ET}}$	211.1	1.09-0.40AI_K+0.32BFI -0.34$AI_{EP}\cancel{AI_{ET}}$	-0.133	-
	GA_M5	IAR	218.3	1.09-0.47IAR	-0.133	-
	GA_M6	AI_K, IAR, BFI, $AI_{EP}\cancel{AI_{ET}}$	207.0	1.09-0.30AI_K-0.27IAR+0.32BFI-0.23$AI_{EP}\cancel{AI_{ET}}$	-0.133	-
Xianyang						
	GA_M0	-	285.8	1.59	-0.184	-
	GA_M1	t	270.1	1.59-0.48t	-0.184	-
	GA_M2a	T	270.1	1.59-0.50T	-0.184	-
	GA_M2b	IAR	267.8	1.59-0.50IAR	-0.184	-
	GA_M3	T, P	267.1	1.59-0.34T+0.32P	-0.184	-
	GA_M4	T, P, BFI, K	265.4	1.59-0.33T+0.27P+0.22BFI+0.18K	-0.184	-
	GA_M5	IAR	267.8	1.59-0.50IAR	-0.184	-
	GA_M6	IAR, $AI_{EP}\cancel{AI_{ET}}$, BFI	259.7	1.59-0.28IAR-0.36 $AI_{EP}\cancel{AI_{ET}}$+0.26BFI	-0.184+0.23IAR	-